

Published in final edited form as:

Biomacromolecules. 2009 June 8; 10(6): 1324–1330. doi:10.1021/bm900189x.

Filamentous polymer nanocarriers of tunable stiffness that encapsulate the therapeutic enzyme catalase

Eric A. Simone^{1,2,3,*}, Thomas D. Dziubla^{2,4}, Dennis E. Discher^{1,2,5}, and Vladimir R. Muzykantov^{2,3,6}

¹Department of Bioengineering, University of Pennsylvania, Philadelphia, PA 19104

²Inst. for Translational Medicine and Therapeutics, University of Pennsylvania, Philadelphia, PA 19104

³Inst. for Environmental Medicine, University of Pennsylvania School of Medicine, Philadelphia, PA 19104

⁴Department of Chemical and Materials Engineering, University of Kentucky, Lexington, KY. 40506

⁵Department of Chemical and Biomolecular Engineering, University of Pennsylvania, Philadelphia, PA 19104

⁶Department of Pharmacology, University of Pennsylvania School of Medicine, Philadelphia, PA 19104

Abstract

Therapeutic proteins are prone to inactivation by aggregation, proteases and natural inhibitors, motivating development of protective delivery systems. Here we focus on protective encapsulation of the potent antioxidant enzyme, catalase, by filamentous polymer nanocarriers (*f-PNC*), with the specific goal of addressing whether polymer molecular weight (MW) controls formation and structural properties such as size and stiffness. While maintaining the same MW ratio of polyethylene glycol (PEG) to polylactic acid (PLA), a series of PEG-b-PLA diblock copolymers were synthesized, with total MW ranging from about 10 kg/mol to 100 kg/mol. All diblocks formed *f-PNC* upon processing, which encapsulated active enzyme that proved resistant to protease degradation. Further, *f-PNC* stiffness, length, and thickness increased with increasing MW. Interestingly, heating above a polymer's glass transition temperature (<30°C) increased *f-PNC* flexibility. Thus we report here for the first time *f-PNC* that encapsulate an active enzyme with polymer MW-tunable flexibility, offering several potential therapeutic applications.

1. Introduction

Non-spherical geometry carriers represent a rapidly growing field in drug delivery. Shapes such as elliptical disks,^{1, 2} carbon nanotubes,³⁻⁵ and filamentous micelles (filomicelles, or worm micelles)^{6, 7} have many potential benefits relative to their spherical counterparts. In particular, filamentous nanocarriers such as filomicelles are flexible and have very similar morphologies to several filamentous viruses found in nature, such as influenza, bird flu, or ebola.⁸⁻¹⁰ Furthermore, this flexible nature can potentially impart several unique features,

*Address for correspondence: email: E-mail: esimone@seas.upenn.edu, phone: 215-898-2449.

Supporting Information Available. A detailed description of polymer synthesis, characterization and formulation into carriers is included in the supplement. This section also contains details of catalase loading within *f-PNC* and subsequent resistance to protease degradation. This information is available free of charge via the Internet at <http://pubs.acs.org>.

including flow alignment, minimization of vascular collision and phagocytosis, and thus enhanced circulation times *in vivo*.⁷ In addition to applications in drug delivery, nanofilaments of varying stiffness have other biomedical applications, such as scaffolding. For instance, ultrafine scaffold materials of lactide and chitosan were synthesized via electrospinning for scaffold tissue engineering applications.¹¹ Similarly, collagen was electrospun into ~100 nm cross sectional diameters and formed into scaffolding mats.¹²

Since filomicelles are self-assembled micellar structures with relatively solid hydrophobic cores, they are ideal for loading of small molecular weight (MW), lipophilic drugs such as taxol.^{7, 13, 14} In a recent study, we found that control of a diblock copolymer's amphiphilicity, through tuning of the ratio of hydrophobic to hydrophilic domains, led to nanocarrier morphology control in an alternative, modified emulsion formulation.¹⁵ Specifically, spheroid or filamentous polymer nanocarriers, *PNC* or *fPNC*, respectively, were formed with what are believed to be interior aqueous domains, unique to this formulation. Within these domains, the relatively hydrophilic and highly potent, yet labile 250 kDa antioxidant enzyme, catalase was not only encapsulated, but resistant to external proteolytic degradation upon *PNC* or *f-PNC* loading. It should be noted that this class of carrier is not designed for traditional “drug release”, but rather serves as a protective cage wherein the enzyme substrate, H₂O₂, is readily diffusible through the polymer shell. These carriers were made from degradable polyether-b-polyester polymers, namely polyethylene glycol-b-poly(lactide) acid, or PEG-PLA.

The goal of this study was to develop enzyme-loaded *f-PNC* with tunable features including stiffness and length. In order to accomplish this, we tested two hypotheses. The first was that PEG-PLA diblock copolymers of comparable composition to those that formulated *f-PNC* in previous studies, regardless of absolute MW, will still form filamentous carriers loaded with active catalase when a modified double emulsion formulation is utilized. The second hypothesis was that modulation of the absolute polymer MW will dictate mechanical properties of the carriers such as flexibility, or stiffness, as well as overall length. Filomicelles have some of these same dependencies on polymer molecular size,^{16, 17} and thus it was plausible that such a phenomenon would translate over to enzyme-loaded *f-PNC* composed of different biodegradable polymers. In this paper we indeed show for the first time development of a battery of different *f-PNC* with controllable physical features, all dependent on the polymer MW. Further, these carriers encapsulated an active, therapeutic enzyme, which was subsequently resistant to external protease degradation.

2. Materials and Methods

2.1. Reagents

All chemicals and reagents were purchased from Sigma-Aldrich (St Louis, MO) and used as received unless otherwise stated. 1,900 and 5,000 molecular weight (MW) methoxy-polyethylene glycol (mPEG) were purchased from Polysciences (Warrington, PA). 10,900 and 19,000 MW mPEG were acquired from Polymer Source (Dorval, Quebec, Canada). Catalase from bovine liver was purchased from Calbiochem (EMD Biosciences, San Diego, CA). Unless noted otherwise, all phosphate buffered saline (PBS) solutions were 20 mM concentration (2.839 grams dibasic sodium phosphate per liter of deionized water, titrated to 7.4 pH with monobasic sodium phosphate, with 9 grams of NaCl per liter).

2.2. Synthesis of diblock copolymers

Polymerizations were performed as previously described¹⁵ and are more thoroughly outlined in the supplement. Briefly, purified lactide was mixed with different MW mPEG in stoichiometric ratios to achieve desired molecular weights via a tin catalyzed ring opening

polymerization (ROP). Number average molecular weights (\bar{M}_n) of purified bulk copolymers were determined using proton nuclear magnetic resonance ($^1\text{H-NMR}$). The weight average molecular weights (\bar{M}_w) and polydispersity indices (PDI) were also determined by gel permeation chromatography (GPC).

The glass transition (T_g) and melt temperature (T_m) thermal properties of the bulk polymer material were determined with a differential scanning calorimeter (DSC 2010, TA Instruments, New Castle, DE). 10 mg polymer samples were crimped inside of standard non-hermetic aluminum pan/lid pairs (TA Instruments). An empty pan of the same material was used for the reference. Samples placed in the DSC were cooled to approximately -70°C while under nitrogen. Subsequently, samples were heated to 120°C at $20^\circ\text{C}/\text{min}$. The heat flow data was plotted against temperature. As the sample was heated from -70°C , after thermally stabilized (no endo/exothermic events, typically before the sample reached -60°C) the T_g was taken as the mid-point of the first endotherm, while the T_m was the minimum of the second endotherm.

2.3. Nanoparticle formation and enzyme encapsulation characterization

A freeze-thaw double emulsion solvent evaporation technique was used as previously outlined^{15, 18} and is described in detail in the supplement. This formulation method was utilized to encapsulate the therapeutic enzyme catalase. Enzyme loading was determined via isotope tracing and enzymatic activity. *f-PNC*-encapsulated catalase resistance to proteolysis was determined via radioisotope tracing of protein loaded within carriers after incubation with the non-specific protease, pronase, as described previously.^{15, 18} Furthermore, a colorimetric PEG assay based on the PEG-Barium Iodide complex was utilized to determine *PNC* concentration.¹⁵ All methods in section 2.3 are outlined in detail in the supplement.

2.4. PNC fluorescence and electron microscopy

PNC morphology was characterized by fluorescence microscopy and transmission electron microscopy (TEM) techniques. For fluorescence microscopy, aliquots of *PNC* were stained with the lipophilic carbocyanine dye, PKH26, via established methods.^{15, 16} Images were taken in real time with an inverted epifluorescence microscope (TE2000-U Eclipse, Nikon Instruments, Inc., Melville, NY) equipped with a 60X oil immersion objective, in conjunction with a UV lamp (Lambda DG-4, Sutter Instrument Co., Novato, CA) and a CCD camera (ORCA-ER C4742, Hamamatsu Corporation, Bridgewater, NJ). For TEM, samples were prepared as previously described.¹⁵ Samples were immobilized on TEM mesh grids (Formvar Film 200 Mesh, Electron Microscopy Sciences, Hatfield, PA). Staining was not necessary for visualization. Grids were imaged on a TEM (JEOL JEM-100CX, West Chester, PA) with an accelerating voltage set to 80 keV.

2.5. PNC persistence length, contour length, and effective length determination

Persistence and contour lengths were determined via established fluorescence techniques^{16, 17} that utilized carriers stained with PKH26. Metamorph imaging software was used for time-lapse image acquisition. The corresponding stack files were exported in AVI format before analysis with ImageJ (NIH). Slides were treated with silicone (SigmaCote[®], Sigma) to minimize non-specific immobilization of *PNC* on the glass. Thermal dependence microscopy studies were performed with a temperature stage (PDMI-2 Open Perfusion Micro-Incubator, Harvard Apparatus, Holliston, Massachusetts) and controller (TC-202A Temperature Controller, Harvard Apparatus). The stage contained 50 μl aliquots of *PNC* samples, confined to a pseudo two-dimensional plane between two cover slips.¹⁶

Effective length was determined via dynamic light scattering (DLS, 90Plus Particle Sizer, Brookhaven Instruments, Holtsville, NY). Diffusion coefficients were determined from the light scattering intensity measurements of the DLS. These diffusion coefficients were used to calculate the effective length via the Stokes-Einstein equation, modified to approximate rod-like structures.^{13, 19}

3. Results

3.1. Polymer characterization

Ring-opening polymerization (ROP) of lactide with different MW monomethoxy-capped mPEG initiators (between 1,900 and 19,000 g/mol) yielded diblock mPEG-b-PLA polymers with total MW's ranging from approximately 12,000 to 89,000 g/mol (see Table 1) as determined by ¹H-NMR. The GPC-determined polydispersity indices of the polymers were between 1.5 and 1.7, typical of ROP products. Names of the individual polymers utilized throughout this paper are also indicated in Table 1. The first two letters indicate the polymer (e.g., EL refers to PEG-PLA) and the second two numbers refer to each polymer block's molecular weight, in kg/mol (e.g., EL2-10 refers to 2 kg/mol PEG-block-10 kg/mol PLA). PLA MW was controlled via the stoichiometry of the reaction, i.e., control of the feed ratio of lactide and mPEG reagents determined the ultimate polymer block MW's. The resultant wt% PLA, or “% PLA”, defined as the ratio of PLA MW to the total diblock MW, is also shown in Table 1. The target PLA fractions were determined based off of previous results that suggested these compositions might formulate filamentous *PNC* (*f-PNC*) loaded with active catalase when a w/o/w freeze-thaw modified double emulsion formulation was utilized.¹⁵

Thermal properties of bulk, dry synthesized polymers (no enzyme) were determined via differential scanning calorimetry (DSC, Fig. 1). Heat flow curves for each polymer are shown, each on the same scale, but offset from one another for the sake of clarity. In a common experiment, a reference cell and sample cell are both heated at a constant rate of temperature increase (e.g., 20°C/min). The difference in heat flow between the sample cell and reference cell are then related to the difference in heat capacity and thermal changes in the sample chamber. As expected for these materials, only two thermal events were observed for each of the scanned polymers, namely the glass transition temperature (T_g) and the melt temperature (T_m). The first observed endotherm indicated that the T_g was just above 25°C for all of the tested polymers. The second endotherm indicated that the T_m of the polymers ranged from 43°C to 53°C. There did not appear to be a clear MW dependence of these thermal properties of the tested diblock copolymers, most likely due to the convoluting inclusion of different MW PEG blocks in each of these copolymers. PEG is a known plasticizer and inclusion of which has profound impacts on material thermal properties such as T_g 's.²⁰ No exothermic events, such as crystallization temperatures (T_c) were noted with any of the polymers.

3.2. PEG-PLA diblocks of similar composition form filamentous PNC with MW and temperature dependent stiffness

The above described polymers were formulated into catalase-loaded nanocarriers with a w/o/w freeze-thaw modified double emulsion, a somewhat more complicated formulation than other typical approaches to making filamentous polymer drug carriers, e.g., film-casting-rehydration self-assembly. The primary benefit of this technique is the potential for active enzyme encapsulation, due to aqueous domain inclusions present with the modified emulsion, yet absent in traditional self-assembled (solid-core) filament micelle structures.^{15, 18} All four tested polymers indeed formed filamentous polymer nanocarriers (*f-PNC*), as verified by fluorescence and electron microscopy, examples of which are shown later in Figures 2 and 4. While the shape was similar between different polymer MW *f-PNC*, several unique physical properties were observed. First and foremost, there was a MW and temperature sensitivity of

the *f-PNC* flexibility, as noted by dynamic light scattering (DLS) experiments, Fig. 2A. Diffusion coefficients of the samples were measured by DLS and the effective lengths were thus determined from a modified Stokes-Einstein equation for diffusion:

$$D = \frac{k_B T}{2\pi\eta L_{\text{Eff}}} \quad (\text{i})$$

where D is the diffusion coefficient, k_B is the Boltzmann constant, T is the sample temperature, η is the temperature-dependent viscosity (predicted by the Brookhaven DLS), and L_{Eff} is the effective length.^{13, 19}

Equation (i) was derived initially to predict the effective length of rigid rods, but has been suitable enough for the approximation of effective lengths of flexible filaments.^{16, 17} While the absolute values are not necessarily the most indicative of the actual *f-PNC* hydrodynamic radii (due to limitations in measurements of non-spherical particles by DLS) relative trends between different filamentous preparations are possible.¹⁵ A built-in heating stage in the DLS provided sample temperature control. At 25°C (Fig. 2A, top curve, white squares) the L_{Eff} increases with MW from 873.7±30.1 nm for EL2-10 to 3028.8±397.9 nm for EL19-70. When the temperature is increased above the T_g of the polymer materials to 37°C (Fig. 2A, bottom curve, black circles), the effective length decreases for all preparations. The overall trend is one of increasing L_{Eff} with increasing MW, where EL2-10 is 838.6±41.9 nm and EL19-70 is 2375.4±690.4 nm. However, it should be noted that there exists a physical limitation of the utilized DLS, where the most reliable measurements are those made of particles (of these particular polymers) with effective sizes less than two to three microns. Gravitational effects and thus sedimentation interfere for larger particles, violating the random-diffusion assumption of DLS.²¹

In order to find a more robust stiffness measurement, we utilized a fluorescence-based technique to quantify the *f-PNC*'s persistence lengths, l_p , where a shorter l_p correlates to a more flexible carrier while longer l_p correlates to a stiffer carrier. l_p is related to the contour length, L , and R , the end-to-end distance of a filament, by the following equation:

$$\langle R^2 \rangle = 2l_p^2 \left[\frac{L}{l_p} - 1 + \exp\left(-\frac{L}{l_p}\right) \right] \quad (\text{ii})$$

where l_p is divided by two due to the pseudo two dimensional confinement of the *f-PNC* sample between coverslips.^{16, 17, 22, 23} Measurements were made from time-lapse fluorescence microscopy images. A few sample fluorescence microscopy frames for EL2-10 *f-PNC* are shown, Fig. 2B. In order to illustrate the degree of fluctuation in conformation of these carriers, ten superimposed backbone traces taken from images at 0.5 second intervals at 25°C are displayed in the inset of Fig. 2C. At 25°C, as MW is increased there is an increase in l_p from 0.9±0.3 μm for EL2-10 to 14.0±2.9 μm for EL19-70, Fig. 2C top curve. In other words, higher MW *f-PNC* are stiffer than lower MW carriers, and l_p follows a power law dependence on MW of $l_p = 0.0011 * MW^{2.1}$ at 25°C. This MW dependent increase in l_p is still observed when the temperature is raised above the T_g of the polymers to 37°C, however the absolute value of the persistence length is reduced for all preparations, Fig. 2C bottom curve. At this temperature, l_p still increased with increasing polymer MW from 0.6±0.09 μm to 1.8±0.5 μm for EL2-10 and EL19-70, respectively and followed the relationship of $l_p = 0.2 * MW^{0.5}$.

3.3. f-PNC contour lengths and cross-sectional diameters are MW dependent

While the general filamentous shape was similar among the synthesized, catalase-loaded PNC, specific physical properties such as the length and thickness of the carriers differed significantly. The contour length, L , of a nanofilament is defined here as the absolute length as traced along its backbone, Fig. 3. Histograms of each different polymer sample show the Gaussian distribution of L for EL2-10 and EL10-40, Fig. 3A,C. The histograms for EL5-27 and EL19-70 were somewhat Gaussian, but due to the outlier length populations Lorentzian distributions provided better fits, Fig. 3B,D. Interestingly, the trend of the average of each preparation is an increase in contour length with increasing polymer MW, Fig. 3E. The shortest L occurs with EL2-10 (12.1 kg/mol) at approximately $4.4 \pm 0.3 \mu\text{m}$ and is maximal at $12.6 \pm 0.9 \mu\text{m}$ for EL19-70 (89.1 kg/mol). This MW dependence of L appears to reach a plateau with increasing MW, similar to a Hill adsorption isotherm. A classic example of such an isotherm depicts that a molecule's (e.g., polymer) concentration, when increased in a solution, is accompanied by an increase in its adsorption onto a surface (e.g., surfactant micelle), ultimately reaching a plateau.^{24, 25} Thus in the *f-PNC* example, the concentration analogue would be polymer MW and the adsorption analogue would be L . In other words, increasing polymer MW increases adsorption of polymer mass onto *f-PNC*, increasing the nanocarriers' contour length, L . This can be approximated by a Hill model of the form^{24, 26}:

$$L = \frac{a \cdot MW^b}{c^b + MW^b}$$

with $a = 12.7$, $b = 2.1$, and $c = 16.1$, from curve-fitting the contour length data. Since b is greater than unity, this implies that there may be cooperative binding of polymer material to nanocarriers during formulation, as polymer MW is increased.^{24, 26} This notion of increased polymer adsorption is somewhat reflected in the *f-PNC* mass yield, Fig. 3E inset, described below.

Quantitative analysis of PEG content from a colorimetric assay revealed the final *f-PNC* mass yield in the nano-scale fraction of the particles. From the following equation based on the equimolar existence of PEG and PLA in the polymer diblock:

$$\text{Diblock polymer mass yield} = \left\{ \frac{x(\text{g, PEG})}{MW_{\text{PEG}}(\text{g/mol, PEG})} \times [MW_{\text{PLA}}(\text{g/mol, PLA})] \right\} + [x(\text{g, PEG})]. \quad (\text{iii})$$

From equation (iii), *f-PNC* mass yield, and thus concentration, was determined. There was an increasing trend in yield with increasing MW, although this seemed to plateau for the highest MW polymers, Fig. 3E inset. The lowest yield was from EL2-10 PNC at $6.0 \pm 0.6 \text{ mg/ml}$, while the highest yield occurred with the polymer EL19-70 at $10.7 \pm 1.4 \text{ mg/ml}$.

Electron micrographs of the different catalase-loaded nanocarrier preparations further verified the PNC's filamentous structure, Fig. 4A. The different MW nanofilaments were free of branching and no spherical population was detected. In this sense, they were relatively homogeneous, but there were distinct differences evident from electron microscopy. Specifically, from the TEMs, line scans across the *f-PNC* revealed their cross sectional diameters increased with increasing MW, although this phenomena appeared to be nearing saturation as the two highest polymer MWs were obtained, Fig. 4B. The narrowest filaments were from polymer EL2-10 with cross sectional diameters, d , of approximately $26.8 \pm 1.4 \text{ nm}$. EL19-70 revealed the widest *f-PNC* with cross sections of $121.1 \pm 3.6 \text{ nm}$.

3.4. Polymer filaments of different MW load active enzyme that is resistant to protease degradation upon encapsulation

Loading of catalase into *f-PNC* and subsequent enzymatic activity was characterized, along with the resistance of the enzyme to degradation by proteases, via established methods¹⁵ and are discussed in detail in the supplement. It is important to note that all filamentous preparations loaded comparable amounts of catalase, relative to previous filament loading efficiencies.¹⁵ However, the loading dependencies on polymer MW were inversely related. Similarly, formulation-induced catalase inactivation, i.e., retention of enzymatic activity post-preparation of the nanofilaments, was similar for each polymer MW, and was relatively mild compared to previous formulations.¹⁵

Assessment of resistance of the encapsulated enzyme to protease (e.g., pronase) degradation represents another means to quantify the quality of catalase encapsulation.^{15, 18, 27} In other words, *f-PNC* protection of catalase helps differentiate truly *encapsulated* drug from drug that is merely surface adsorbed, or near the surface of the particle and potentially susceptible to external protease denaturation. Percent protection, or the amount of protein resistant to protease degradation relative to the total protein loaded into *f-PNC*, was significantly higher than non-*PNC* encapsulated catalase preparations. These results are also detailed in the supplement.

4. Discussion

Particles of anisotropic geometry, such as filamentous or even disk-shaped carriers have several unique features as drug delivery systems.^{2, 7, 13} Despite the nano cross sectional diameters of many of these carriers, namely filaments, their micron scale lengths afford them a tremendous drug loading capacity. In particular, these very same dimensional attributes can, combined with varying degrees of flexibility, enable unprecedented, prolonged circulation residence times in some animal models⁷ and may provide unique paradigms in terms of sub-cellular addressing. Similarly, the fact that these carriers are essentially all *surface* makes them ideal candidates for drug targeting, where site-specific epitopes would be conjugated to their surface.⁶ Therapeutic cargoes could even be loaded via the same mechanism.

In this study, we demonstrate the polymer MW control of two unique features of the particle formulation utilized. First, through maintenance of comparable ratios of hydrophobic to hydrophilic domains in the polymer, regardless of the absolute MW, enzyme-loaded filamentous *PNC* are possible. Second, the above-mentioned parameter of carrier stiffness is MW-tunable, i.e., increasing MW increases *f-PNC* flexibility in solution. Similarly, the contour lengths and cross sectional diameters of the *f-PNC* demonstrated polymer MW dependence, analogous to the MW-stiffness relationship. It should be noted that in addition to polymer MW reduction, sonication can also be utilized to reduce the length of these filamentous carriers, if so desired (data not shown).

The MW-tunable stiffness phenomenon is closely related to the inherent thermal properties of the polymer. As revealed by DSC, the T_g for the polymers tested are all just above room temperature. When heated above the T_g , there is a noticeable increase in carrier flexibility. Initially observed by time-resolved fluorescence microscopy, this effect was mirrored by DLS. Interestingly, the 37°C curves from Figures 3 (fluorescence) and 4B (light scattering), when plotted on the same scale axes, are actually quite similar. Although the trend is increased effective length by DLS with increasing MW at 25°C (Fig. 4B), similar to enhanced persistence length (Fig. 3), the absolute values do not correlate one to one between fluorescence and light scattering measurements. This is potentially due to limitations in the DLS equipment that result from competition with random diffusion by gravity effects such as sedimentation, which we observe for the larger MW *f-PNC*. As can be seen by the fluorescence image analysis-determined persistence lengths in Fig. 3, the most reliable range for DLS (typically less than

two to three microns for carriers of this material) is notably exceeded for higher MW preparations and thus may fall out of range of DLS. Further, as mentioned in the results section, the modified Stokes-Einstein diffusion equation was originally derived to describe rigid rods, not flexible filaments. Regardless, the trends still indicate this unique temperature sensitive property of these enzyme-loaded filaments.

Interestingly, enzyme loading was inversely proportional to polymer MW. Intuitively, one would expect that higher MW *f-PNC*, with thicker cross sectional diameters and longer contour lengths, would load protein more efficiently. Perhaps the greatest insight into this trend comes from the similar result that cargo-protease resistance also decreased with increasing polymer MW. From previous studies, such a phenomenon indicates that the protein is either surface adsorbed onto or loosely associated with the carrier, and thus not protected from external proteases.¹⁵ Although the ratio of PEG to PLA molecular sizes is comparable for all *f-PNC* preparations tested, it is conceivable that at increasingly higher absolute polymer MWs, the degree of hydrophobicity enhancement of PLA and hydrophilicity enhancement of PEG is not 1:1. In other words, it is possible that the higher MW PLA is proportionately more hydrophobic than the higher MW PEG is hydrophilic. Thus there may be tighter packing of the hydrophobic domains, decreasing the internal *PNC* loading capacity of relatively hydrophilic proteins. Surface adsorption of proteins is also somewhat compromised due to the increasingly higher MW PEG chains used. This poses an interesting research question, namely modeling of the molecular assembly of amphiphilic polymers that occur during a complex freeze-thaw double emulsion formulation. The level of complexity would be much higher, relative to simpler self-assembly processes, such as those utilized to form filomicelles.²⁸ This would be a fascinating extension and would make an interesting future study.

Some interesting comparisons can be made with filamentous micelles (filomicelles) made from similar materials but formulated with different techniques.¹⁴ Importantly, it should be noted that the self-assembled filomicelles (AKA worm micelles) in question were prepared with a cosolvent/evaporation technique, while the non-self-assembled carriers (*f-PNC*) in this study were synthesized with a modified double emulsion. Filomicelles can be made from several different amphiphilic diblock copolymers, but perhaps the most appropriate comparison would be with those made from PEG-PCL (polycaprolactone), a polyether-b-polyester, similar to PEG-PLA. One key difference in the material that should be noted is the difference in hydrophobicity; PCL is often considered much more hydrophobic than PLA. Regardless, filomicelles have been shown to have a similar persistence length and cross sectional diameter dependence on polymer MW.¹⁷ Furthermore, PEG-PCL filomicelles, although typically made from lower MW polymers than utilized in this study, do have comparable persistence lengths to the PEG-PLA carriers reported here.¹⁴ For example, a 4.7 kg/mol PEG-PCL filomicelle has an l_p of ~500 nm while a higher MW version, 11.5 kg/mol, registers at ~5 microns. The closest PEG-PLA polymer for comparison from this study would be EL2-10 (~12 kg/mol) which forms filaments with an l_p of ~900 nm, Fig. 3. The much higher PEG-PLA MWs in this study might also explain the notably higher cross-sectional diameters observed, relative to filomicelles. For instance, increasing PEG-PCL MW from 4.7 kg/mol to 11.5 kg/mol resulted in an increase of diameter from ~11 nm to ~29 nm. Similarly, EL2-10 (12.1 kg/mol) *f-PNC* had $d \sim 27$ nm, yet EL19-70 (89.1 kg/mol) had $d \sim 121$ nm, Fig. 4A. Given the similarities between filomicelles and *f-PNC*, it would be interesting to see if similar trends are seen with filomicelles composed of significantly higher polymer MW.

5. Conclusion

This study demonstrates the control of polymer MW on physical properties of active enzyme-loaded filamentous *PNC*. In particular, stiffness, length, and cross sectional diameter can be finely tuned through alterations in the absolute polymer MW. Due to the unique thermal

properties of the polymers utilized for carrier formation, the resultant *f-PNC* are quite flexible at physiologic temperatures. Furthermore, control of the polymer backbone structure enables enzyme-loadable nanofilaments across a broad range of polymer MWs. This offers a new genre of non-spherical enzyme delivery devices with several potential applications both in targeting and sub-cellular addressing.

Supplementary Material

Refer to Web version on PubMed Central for supplementary material.

Acknowledgements

We thank Marc Ilies of Temple University for assistance with NMR studies, and Darren Brey and Jason Burdick of the University of Pennsylvania for assistance with GPC studies. Finally, Karthikan Rajagopal in the laboratory of Dennis Discher at the University of Pennsylvania is graciously acknowledged for reviewing this manuscript. This work was supported by grants from the National Institutes of Health (NIH #'s HL007954, HL073940-01-A1 and PO1-HL079063).

Abbreviations

PNC, polymer nanocarrier; f-PNC, filamentous polymer nanocarrier; PEG, poly(ethylene glycol); PLA, poly(lactic acid); PVA, poly(vinyl alcohol); DCM, dichloromethane; THF, tetrahydrofuran; MW, molecular weight; DSC, differential scanning calorimetry.

References

1. Champion JA, Mitragotri S. Role of target geometry in phagocytosis. *Proc Natl Acad Sci U S A* 2006;103(13):4930–4. [PubMed: 16549762]
2. Muro S, Garnacho C, Champion JA, Leferovich J, Gajewski C, Schuchman EH, Mitragotri S, Muzykantov VR. Control of Endothelial Targeting and Intracellular Delivery of Therapeutic Enzymes by Modulating the Size and Shape of ICAM-1-targeted Carriers. *Mol Ther*. 2008
3. Cato MH, D'Annibale F, Mills DM, Cerignoli F, Dawson MI, Bergamaschi E, Bottini N, Magrini A, Bergamaschi A, Rosato N, Rickert RC, Mustelin T, Bottini M. Cell-type specific and cytoplasmic targeting of PEGylated carbon nanotube-based nanoassemblies. *J Nanosci Nanotechnol* 2008;8(5):2259–69. [PubMed: 18572636]
4. Jin H, Heller DA, Strano MS. Single-Particle Tracking of Endocytosis and Exocytosis of Single-Walled Carbon Nanotubes in NIH-3T3 Cells. *Nano Lett* 2008;8(6):1577–1585. [PubMed: 18491944]
5. Kam NW, Liu Z, Dai H. Carbon nanotubes as intracellular transporters for proteins and DNA: an investigation of the uptake mechanism and pathway. *Angew Chem Int Ed Engl* 2006;45(4):577–81. [PubMed: 16345107]
6. Dalhaimer P, Engler AJ, Parthasarathy R, Discher DE. Targeted worm micelles. *Biomacromolecules* 2004;5(5):1714–9. [PubMed: 15360279]
7. Geng Y, Dalhaimer P, Cai S, Tsai R, Tewari M, Minko T, Discher DE. Shape effects of filaments versus spherical particles in flow and drug delivery. *Nat Nano* 2007;2(4):249–255.
8. Geisbert TW, Jahrling PB. Exotic emerging viral diseases: progress and challenges. *Nat Med* 2004;10(12 Suppl):S110–21. [PubMed: 15577929]
9. Roberts PC, Lamb RA, Compans RW. The M1 and M2 proteins of influenza A virus are important determinants in filamentous particle formation. *Virology* 1998;240(1):127–37. [PubMed: 9448697]
10. Shortridge KF, Zhou NN, Guan Y, Gao P, Ito T, Kawaoka Y, Kodihalli S, Krauss S, Markwell D, Murti KG, Norwood M, Senne D, Sims L, Takada A, Webster RG. Characterization of avian H5N1 influenza viruses from poultry in Hong Kong. *Virology* 1998;252(2):331–42. [PubMed: 9878612]
11. Skotak M, Leonov AP, Larsen G, Noriega S, Subramanian A. Biocompatible and Biodegradable Ultrafine Fibrillar Scaffold Materials for Tissue Engineering by Facile Grafting of L-Lactide onto Chitosan. *Biomacromolecules* 2008;9(7):1902–1908. [PubMed: 18540676]

12. Matthews JA, Wnek GE, Simpson DG, Bowlin GL. Electrospinning of collagen nanofibers. *Biomacromolecules* 2002;3(2):232–8. [PubMed: 11888306]
13. Cai S, Vijayan K, Cheng D, Lima EM, Discher DE. Micelles of Different Morphologies-Advantages of Worm-like Filomicelles of PEO-PCL in Paclitaxel Delivery. *Pharm Res.* 2007
14. Geng Y, Discher DE. Visualization of degradable worm micelle breakdown in relation to drug release. *Polymer* 2006;47(7):2519–2525.
15. Simone EA, Dziubla TD, Colon-Gonzalez F, Discher DE, Muzykantov VR. Effect of polymer amphiphilicity on loading of a therapeutic enzyme into protective filamentous and spherical polymer nanocarriers. *Biomacromolecules* 2007;8(12):3914–21. [PubMed: 18038999]
16. Dalhaimer P, Bates FS, Discher DE. Single molecule visualization of stable, stiffness-tunable, flow-conforming worm micelles. *Macromolecules* 2003;36(18):6873–6877.
17. Dalhaimer P, Bermudez H, Discher DE. Biopolymer mimicry with polymeric wormlike micelles: Molecular weight scaled flexibility, locked-in curvature, and coexisting microphases. *Journal of Polymer Science Part B-Polymer Physics* 2004;42(1):168–176.
18. Dziubla TD, Karim A, Muzykantov VR. Polymer nanocarriers protecting active enzyme cargo against proteolysis. *J Control Release* 2005;102(2):427–39. [PubMed: 15653162]
19. Li G, Tang JX. Diffusion of actin filaments within a thin layer between two walls. *Phys Rev E Stat Nonlin Soft Matter Phys* 2004;69(6 Pt 1):061921. [PubMed: 15244631]
20. Repka MA, Gerding TG, Repka SL, McGinity JW. Influence of plasticizers and drugs on the physical-mechanical properties of hydroxypropylcellulose films prepared by hot melt extrusion. *Drug Dev Ind Pharm* 1999;25(5):625–33. [PubMed: 10219532]
21. Berne, BJ.; Pecora, R. *Dynamic light scattering: with applications to chemistry, biology, and physics.* R.E. Krieger Pub. Co.; Malabar, Fla.: 1990. p. vii-376.
22. Wilhelm J, Frey E. Radial Distribution Function of Semiflexible Polymers. *Phys Rev Lett* 1996;77(12):2581–2584. [PubMed: 10061990]
23. Grosberg, A.Y.; Khokhlov, A.R. *Statistical Physics of Macromolecules.* AIP Press; New York: 1994.
24. Poland, D. *Cooperative equilibria in physical biochemistry.* Clarendon Press; Oxford [Eng.]: 1978. p. x-344.
25. Kwak, JCT. *Polymer-surfactant systems.* M. Dekker; New York: 1998. p. viii-482.
26. Hill AV. The possible effects of the aggregation of the molecules of haemoglobin on its dissociation curves. *J Physiol* 1910;40:iv–vii. *Proceedings of the Physiological Society*: Jan. 22, 1910
27. Dziubla TD, Shuvaev VV, Hong NK, Hawkins BJ, Madesh M, Takano H, Simone EA, Nakada MT, Fisher A, Albelda SM, Muzykantov VR. Endothelial targeting of semi-permeable polymer nanocarriers for enzyme therapies. *Biomaterials* 2008;29(2):215–27. [PubMed: 17950837]
28. Srinivas G, Discher DE, Klein ML. Self-assembly and properties of diblock copolymers by coarse-grain molecular dynamics. *Nat Mater* 2004;3(9):638–44. [PubMed: 15300242]
29. Shuvaev VV, Dziubla T, Wiewrodt R, Muzykantov VR. Streptavidin-biotin crosslinking of therapeutic enzymes with carrier antibodies: nanoconjugates for protection against endothelial oxidative stress. *Methods Mol Biol* 2004;283:3–19. [PubMed: 15197299]
30. Beers RF Jr, Sizer IW. A spectrophotometric method for measuring the breakdown of hydrogen peroxide by catalase. *J. Biol. Chem* 1952;195(1):133–140. [PubMed: 14938361]
31. Sims GE, Snape TJ. A method for the estimation of polyethylene glycol in plasma protein fractions. *Anal Biochem* 1980;107(1):60–3. [PubMed: 7435960]

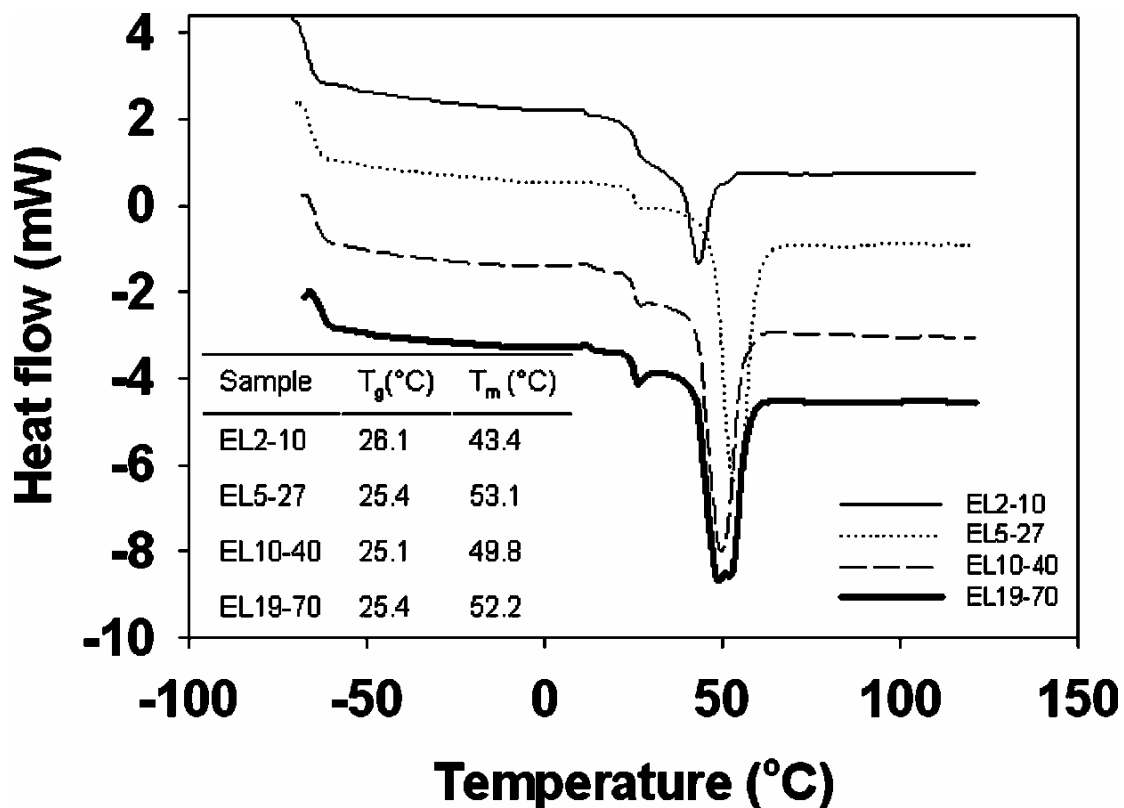


Figure 1. DSC of PEG-PLA polymers

DSC curves of different MW polymers are shown, all on the same scale, but offset from one another for the sake of clarity. Heat flow describes the amount of energy that flows to the polymer sample to maintain it at the same temperature as the reference pan utilized in the DSC. The absolute value of the heat flow curves are not as indicative of the thermal characteristics of the polymers as are the temperatures at which endothermic events occur, indicated in the inset table. The inset table thus lists the glass transition temperature (T_g , from the first endotherm encountered upon sample heating) and melt temperature (T_m , from the second endotherm) of each polymer.

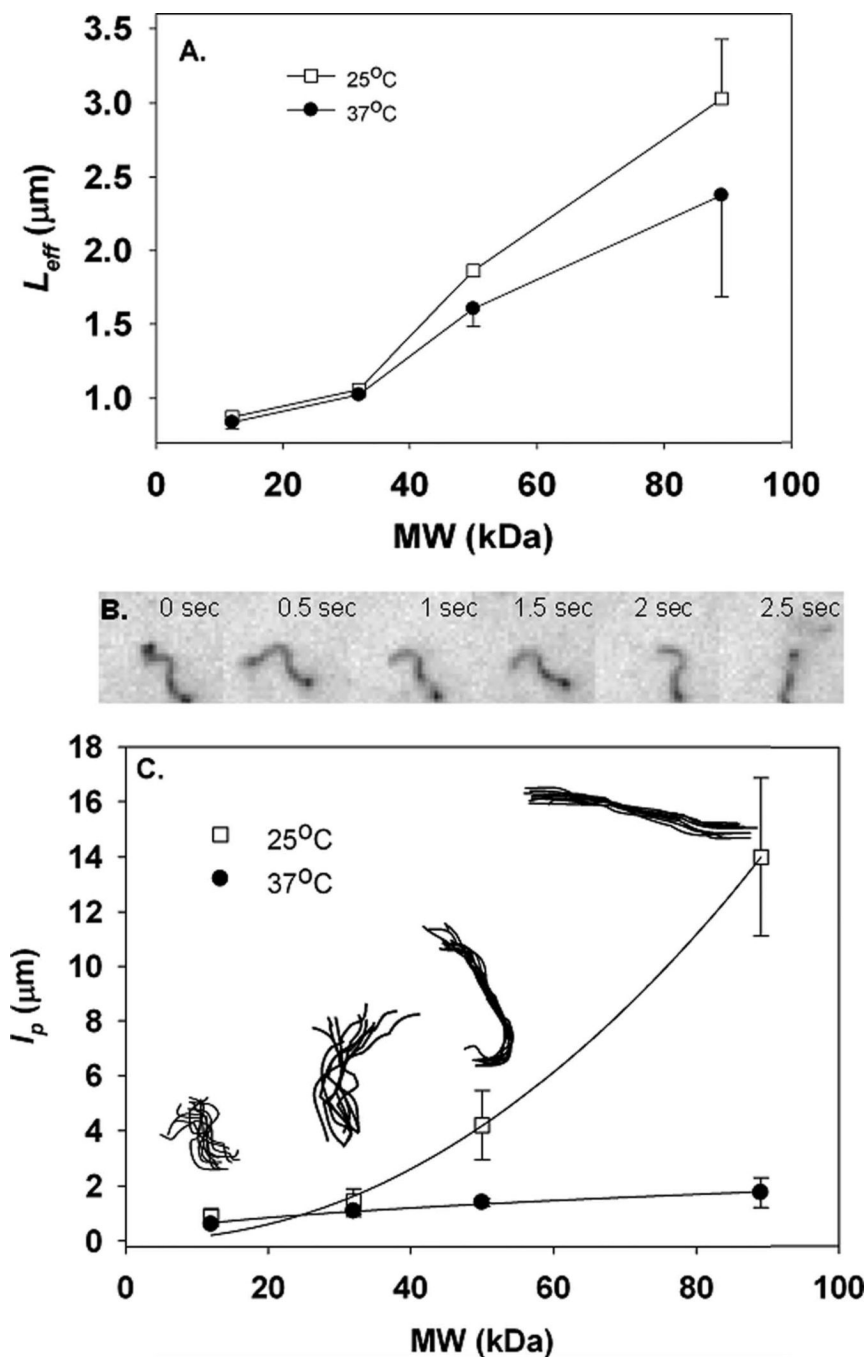


Figure 2. *f*-PNC stiffness is MW and temperature dependent

Effective length, from DLS, is shown as a function of polymer MW (A). DLS built-in heating stage controlled temperature, set below the polymer glass transition temperatures at 25°C (white squares, top curve) or above the glass transition temperatures 37°C (black circles, bottom curve). To overcome the technical limitations of DLS, stiffness, as quantified by persistence length, l_p , was determined from fluorescence time-lapse video analysis (B,C). Higher l_p corresponds to stiffer carriers. Six frames of a sample time lapse (EL2-10 *f*-PNC) are shown (B). The l_p of different preparations are summarized as a function of polymer MW for these catalase-loaded *f*-PNC (C). Results from two different temperatures are shown - (25°C, white squares, top curve and 37°C, black circles, lower curve). Sample backbone traces of

10 consecutive frames, taken at 0.5 second intervals at 25°C, are overlaid and shown for each different MW *f-PNC* preparation (inset, C). All values shown are average±SEM.

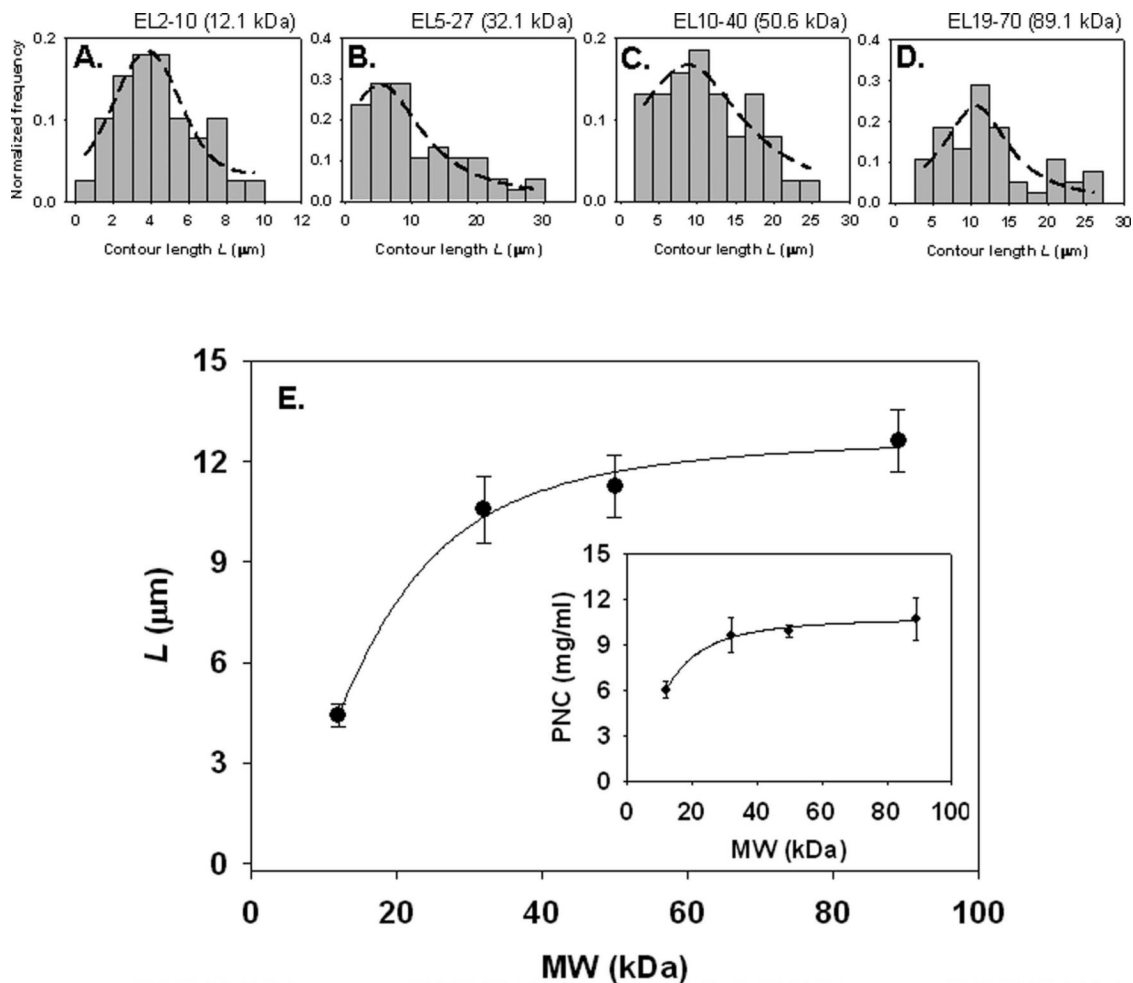


Figure 3. Contour lengths of enzyme-loaded f -PNC are MW dependent
 Mean contour lengths were taken from 40-50 independent measurements of each different MW f -PNC preparation. Contour length is defined as the absolute length, traced along the filament backbone. Histograms indicate the contour length distribution for each preparation (A-D). Dashed lines represent regression equations that best represented the length data. (A) and (C) fit Gaussian distributions. Due to the outlier populations of (B) and (D), Gaussian distributions did not fit as well. Rather these histograms (B and D) were better described by a Lorentzian distribution. A summary of the average contour lengths of each f -PNC, as a function of polymer MW (E) is shown, with a relation similar to a Hill adsorption isotherm. Mass yield concentration of f -PNC by colorimetric assay for polymer content is shown in the inset. All f -PNC preparations were spun down and re-suspended in 1 ml PBS before mass determination. A 100% yield would be 25 mg/ml.

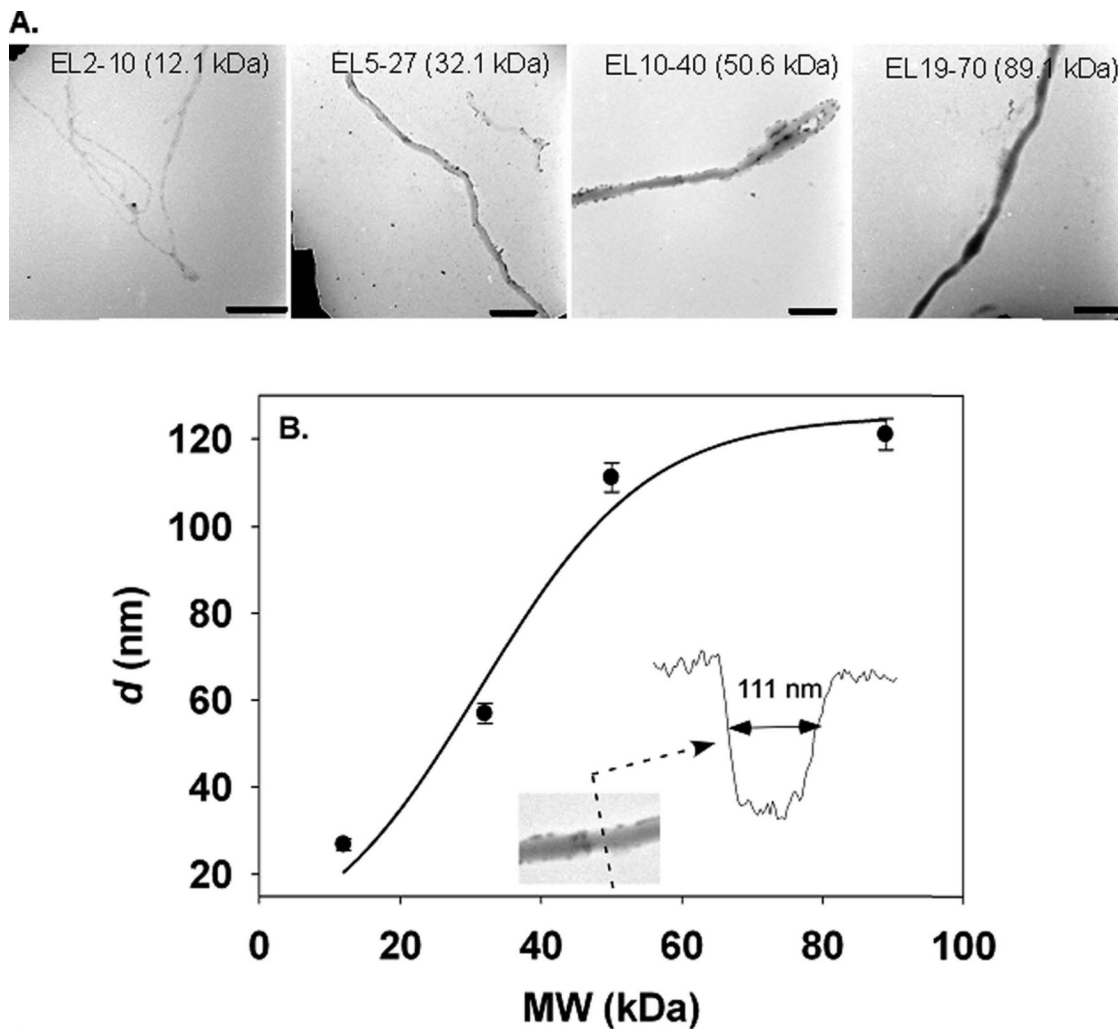


Figure 4. *f*-PNC cross sectional diameter is MW dependent
 Cross sectional diameters, *d*, were determined from TEM image analysis of catalase-loaded *f*-PNC (A). A summary of the *f*-PNC *d* is shown in (B). Inset shows the results of a line scan across an example EL10-40 *f*-PNC. Scale bars are 500 nm.

Synthesized polymer characterization

Table 1

Polymer synthesis results. Number average molecular weights (\bar{M}_n) and polydispersities (PDI). Actual % PLA, or wt% PLA, is defined as the ratio of the actual PLA block \bar{M}_n to the entire diblock copolymer \bar{M}_n . The corresponding MW methoxy end-capped mPEG utilized for each polymer is indicated in the first column. The nomenclature for each polymer is indicated in the last column.

PEG \bar{M}_n (g/mol)	target PLA \bar{M}_n (g/mol)	PLA \bar{M}_n^a (g/mol)	%PLA	Total MW (g/mol)	PDI ^b	Name
1900.0	10000.0	10165.7	84.3	12065.7	1.7	EL2-10
5000.0	30000.0	27091.3	84.4	32091.3	1.6	EL5-27
10200.0	40000.0	40437.0	79.9	50637.0	1.6	EL10-40
19000.0	70000.0	70095.3	78.7	89095.3	1.5	EL19-70

^a determined by ¹H-NMR

^b determined by GPC